Role of Histidine-40 in Ribonuclease T1 Catalysis: Three-Dimensional Structures of the Partially Active His40Lys Mutant[†,‡]

Ingrid Zegers,[*,§] Patrick Verhelst,[§] Hui-Woog Choe,[∥] Jan Steyaert,[§] Udo Heinemann,[∥] Wolfram Saenger,[∥] and Lode Wyns[§]

Instituut voor Moleculaire Biologie, Laboratorium Ultrastructuur, Vrije Universiteit Brussel, Paardenstraat 65, B-1640 St. Genesius-Rode, Belgium, and Institut für Kristallographie, Freie Universität Berlin, Takustrasse 6, D-1000 Berlin 33, Germany

Received December 3, 1991; Revised Manuscript Received May 8, 1992

ABSTRACT: Histidine-40 is known to participate in phosphodiester transesterification catalyzed by the enzyme ribonuclease T1. A mutant enzyme with a lysine replacing the histidine-40 (His40Lys RNase T1) retains considerable catalytic activity [Steyaert, J., Hallenga, K., Wyns, L., & Stanssens, P. (1990) *Biochemistry 29*, 9064–9072]. We report on the crystal structures of His40Lys RNase T1 containing a phosphate anion and a guanosine 2′-phosphate inhibitor in the active site, respectively. Similar to previously described structures, the phosphate-containing crystals are of space group $P2_12_12_1$, with one molecule per asymmetric unit (a = 48.27 Å, b = 46.50 Å, c = 41.14 Å). The complex with 2′-GMP crystallized in the lower symmetry space group $P2_1$, with two molecules per asymmetric unit (a = 49.20 Å, b = 48.19 Å, c = 40.16 Å, β = 90.26). The crystal structures have been solved at 1.8- and 2.0-Å resolution yielding R values of 14.5% and 16.0%, respectively. Comparison of these His40Lys structures with the corresponding wild-type structures, containing 2′-GMP [Arni, R., Heinemann, U., Tokuoka, R., & Saenger, W. (1988) *J. Biol. Chem. 263*, 15358–15368] and vanadate [Kostrewa, D., Hui-Woog Choe, Heinemann, U., & Saenger, W. (1989) *Biochemistry 28*, 7692–7600] in the active site, respectively, leads to the following conclusions. First, the His40Lys mutation causes no significant changes in the overall structure of RNase T1; second, the Lys40 side chains in the mutant structures occupy roughly the same space as His40 in the corresponding wild-type RNase T1 structures. Similar to His40 in the corresponding wild-type structures, the side-chain amino group of Lys40 forms a hydrogen bond with the 2′-GMP phosphate moiety and with the phosphate anion in the His40Lys RNase T1 structures complexed with a 2′-GMP and a phosphate, respectively. Tyr38, Lys40, Glu58, Arg77, and His92, which have been shown to contribute to catalytic turnover, form hydrogen bonds with the 2′-GMP phosphate moiety in the His40Lys RNase T1·2′-GMP complex. The intermolecular interactions of Arg77 and His92 were not observed in the corresponding wild-type RNase T1·2′-GMP complex. This difference may be correlated with a change in sugar pucker; in the His40Lys RNase T1·2′-GMP structure, the 2′-GMP inhibitor adopts a C3′-endo-syn conformation, whereas the 2′-GMP sugar pucker is C2′-endo in the corresponding wild-type complex. All crystallographic results are consistent with an ancillary role of the His40 side chain in RNase T1 catalysis; Lys40 of His40Lys RNase T1 can contribute to catalysis by the activation of the phosphate diester and the electrostatic stabilization of the pentacovalent phosphorane transition state.

Ribonuclease T1 (EC 3.1.27.3) from the fungus *Aspergillus oryzae* is the best known representative of a family of homologous microbial ribonucleases (Hill et al., 1983). RNase T1[1] cleaves P–O5′ ester bonds in single-stranded RNA, specifically at the 3′-phosphate of guanylic acid residues (Sato & Egami, 1957). The first step in the reaction is a transesterification and results in a 2′,3′-cyclic quanosine phosphate, which in a second step may be hydrolyzed to yield 3′-guanylic acid. Eckstein et al. (1972) showed the stereochemistry of the transesterification step to follow a concerted in-line mechanism, requiring general-base catalysis toward the 2′-OH and general-acid catalysis toward the leaving 5′-O, by two distinct functional groups located on either side of the scissile bond (Usher, 1969).

Based on the crystal structure of RNase T1 complexed with the specific inhibitor 2′-GMP and early spectroscopic and kinetic data, Heinemann and Saenger (1982, 1983) proposed a mechanism in which Glu58 and His92 act as general base and general acid, respectively. This model was challenged by Nishikawa et al. (1987), who observed high residual activities for Glu58Ala RNase T1. They proposed a mechanism in which two histidines (His40 and His92) act as general base and general acid, as is the case in bovine ribonuclease A. A recent pH-dependence study on RNase T1 mutants (Steyaert et al., 1990) favors the assignment of the role of the base catalyst to Glu58. It was proposed that the protonated His40 imidazole participates in electrostatic stabilization of the transition-state intermediate. Consistent with the fact that lysine resembles a protonated histidine through its positive charge, the His40Lys mutant of RNase T1 was observed to

[†] This work was supported by the Vlaams Actieprogramma Biotechnologie, the Deutsche Forschungsgemeinschaft, the Fonds der Chemischen Industrie, and NATO (Grant 900270). I.Z. is recipient of a grant from the Instituut voor Wetenschappelijk Onderzoek in de Nijverheid en de Landbouw. P.V. and J.S. are research assistants of the Nationaal Fonds voor Wetenschappelijk Onderzoek.

[‡] Crystallographic coordinates have been submitted to the Brookhaven Protein Data Bank. The entry numbers are as follows: His40Lys RNase T1·2′-GMP, PDB1AAD.ENT; His40Lys RNase T1·phosphate, PDB1AAE.ENT.

[§] Vrije Universiteit Brussel.

[∥] Freie Universität Berlin.

[1] Abbreviations: 2′-GMP, guanosine 2′-phosphate; 2′,5′-GpG, guanylyl-2′,5′-guanosine; MPD, 2-methyl-2,4-pentanediol; PEG, poly(ethylene glycol); RNase T1, *Aspergillus oryzae* ribonuclease T1; rms, root mean square deviation; 3′,5′-UpU, uridyl-3′,5′-uridine.

0006-2960/92/0431-11317$03.00/0

Table I: Details about Crystallization, Data Collection, and Refinement

	His40Lys RNase T1·2′-GMP	His40Lys RNase T1·phosphate
crystallization conditions	sitting drop vapor diffusion 10 mg/mL protein in 20 mM sodium acetate, 2 mM calcium acetate, 0.2% (w/v) 2′-GMP, pH 4.2	sitting drop vapor diffusion 20 mg/mL protein in 20 mM Tris acetate, 5 mM sodium acetate, 2 mM calcium acetate, pH 7
precipitant	53% (v/v) MPD	40% (w/v) PEG 4000
space group	$P2_1$	$P2_12_12_1$
cell parameters		
a (Å)	49.20	48.27
b (Å)	48.16	46.50
c (Å)	40.19	41.12
β (deg)	90.26	
data collection	STOE four circle diffractometer, Ni-filtered Cu Kα, fine focus X-ray tube, 40 kV, 35 mA	Turbo-CAD4 diffractometer, Ni-filtered Cu Kα, FR571 rotating anode, 45 kV, 99 mA
resolution (Å)	2	1.8
R_{sym}[a]	0.093	0.063
completeness of last resolution shell (Å)	2.0–2.3 (77%)	1.8–2 (77%)
total no. of reflections (I/σ)	(1) 11 096 (2) 10 967 (3) 10 653	(1) 6928 (2) 5986 (3) 5371
initial model	Arni et al. (1988)	Martinez-Oyanedel et al. (1991)
no. of water molecules in the asym unit of the final structure	239	115
final R factor (%)	16.0	14.5
rms deviation of bond lengths[b] (Å)	0.023 (0.020)	0.018 (0.020)
rms deviation of angles[b] (Å)	0.056 (0.050)	0.056 (0.050)
rms deviation from plane[b] (Å)	0.012 (0.015)	0.010 (0.015)
rms deviation from chiral volume[b] (Å)	0.163 (0.150)	0.131 (0.150)

[a] $R_{sym} = \sum_i\sum_j|\langle I_i\rangle - I_{i,j}|/\sum_i\sum_j I_{i,j}$, summation over j multiple intensities in i unique reflections. [b] The value in parentheses is the target variance used in the refinement. The weight applied to the corresponding restraint is the inverse square of the target value.

retain 3.1% of the wild-type activity, whereas His40Ala and His40Asp RNase T1 retain less than 0.1% of the wild-type activity.

We have investigated the structural implications of the mutation of His40 to lysine by X-ray crystallography. The results further support the hypothesis that the Glu58–His92 pair represents the required base–acid couple and that His40 stabilizes the pentacovalent phosphorane transition state electrostatically.

EXPERIMENTAL PROCEDURES

Crystallization and Data Collection. The production and purification of His40Lys RNase T1 have been described previously (Steyaert et al., 1990). The enzyme was crystallized under two different conditions. The crystallization conditions and details about data collection are described in Table I. In the first case, the mutant enzyme was crystallized without 2′-GMP inhibitor at pH 7.0. These crystals of space group $P2_12_12_1$ were almost isomorphous to the wild-type enzyme crystals obtained under the same crystallization conditions (Martinez-Oyanedel et al., 1991). In the second case, the mutant enzyme was cocrystallized with 2′-GMP at pH 4.2 (His40Lys RNase T1·2′-GMP). In contrast to previously published RNase T1 crystals which were orthorhombic (Pace et al., 1991), these crystals are monoclinic ($P2_1$). Indeed, precession photographs of the His40Lys RNase T1·2′-GMP crystals showed several weak axial reflections which should be systematically extinguished in $P2_12_12_1$ and no *mm* symmetry for the *h0l* projections was observed. Merging the diffraction data into an octant of reciprocal space gives a $R_{sym} = \sum_i\sum_j|\langle I_i\rangle - I_{i,j}|/\sum_i\sum_j I_{i,j} = 0.302$, demonstrating that the two halves of the merged data set are not equivalent.

Refinement. The structures of the mutant RNase T1 molecules were determined by molecular replacement starting from near-isomorphous model structures. The structure of inhibitor-free wild-type RNase T1 (Martinez-Oyanedel et al., 1991) was used as a model for the guanosine-free His40Lys RNase T1. The wild-type RNase T1·2′-GMP structure [$P2_12_12_1$, with one molecule per asymmetric unit (Arni et al., 1988)] was used as a model for His40Lys RNase T1·2′-GMP ($P2_1$). The near-identical cell constants and the orthorhombic pseudosymmetry indicate that the unit cell of the monoclinic His40Lys RNase T1·2′-GMP crystals also contains four molecules, now with two molecules per asymmetric unit. The unit cell contents of the wild-type complex (Arni et al., 1988) were transformed from the orthorhombic to the monoclinic system through a translation of the origin and a (010, 100, 00–1) rotation. All non-protein atoms and the His40 imidazole were removed from the model structures prior to refinement.

For both crystals the model molecules were oriented in the asymmetric unit with rigid body refinement using the program CORELS (Sussman et al., 1977). The structures were refined by stereochemically restrained least-squares refinement using the fast Fourier transform version PROFFT (Finzel, 1987; Sheriff, 1987) of the program PROLSQ (Hendrickson & Konnert, 1980; Hendrickson, 1985). The least-squares refinement was combined with manual model revisions, using the computer graphics program FRODO (Jones, 1978, 1985) on the vector graphics system Evans & Sutherland PS390.

The side chain of Lys40, the water molecules, and the calcium ion were fitted into difference electron densities; the 2′-GMP inhibitor was fitted manually into the His40Lys RNase T1·2′-GMP complex. In the active site of guanosine-free RNase T1, a difference density indicated the presence of a tetrahedral anion. As phosphate buffers were used during the purification of the protein, this anion was assumed to be a phosphate. Hydrogen bonds were identified following the criteria of Baker and Hubbard (1984).

RESULTS

Structure of the His40Lys RNase T1·2′-GMP Complex

Overall Structure. The final atomic coordinate set contains (1) two His40Lys RNase T1 molecules complexes with 2′-GMP, each consisting of 780 protein atoms, 24 inhibitor atoms, and 1 calcium ion, and (2) 239 symmetry-independent water molecules in fully occupied positions. The atomic coordinates and temperature factors have been deposited in the Brookhaven Protein Data Bank. Figure 1 shows the overall structure of His40Lys RNase T1, molecule 1. Although the crystals of His40Lys RNase T1·2′-GMP belong to the lower symmetry monoclinic space group $P2_1$, the packing of the molecules in

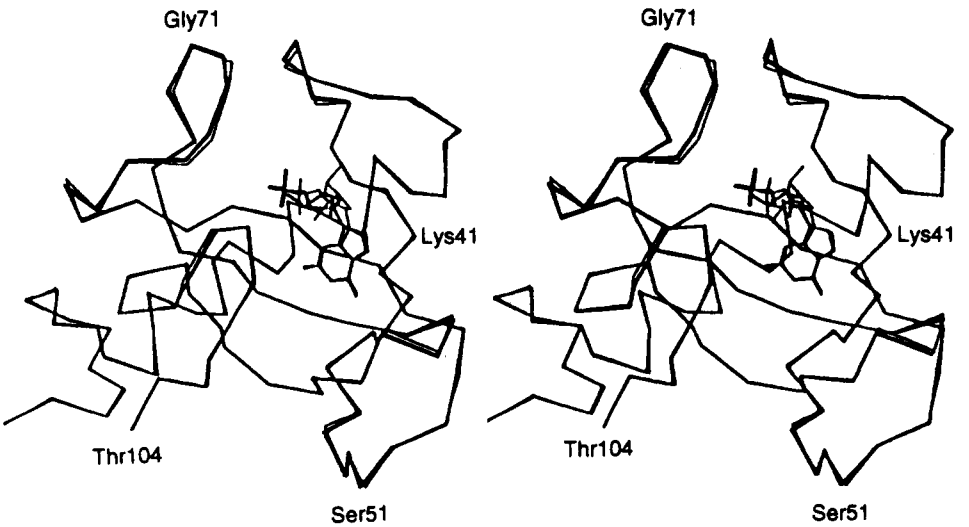

FIGURE 1: Comparison of the structures of wild-type RNase T1 (thin lines) and His40Lys RNase T1 (molecule 1; heavy lines), both complexed with 2′-GMP. The structures were superimposed by matching the α-carbon positions by a least-squares fitting.

Table II: Crystal Contacts[a]

	His40Lys RNase T1·2′-GMP		wt[d] RNase T1·2′-GMP[b]	His40Lys RNase T1·phosphate	wt RNase T1·vanadate[c]
	molecule 1	molecule 2			
Ala1 N–His92 O	2.6	2.9	2.7	3.3	3.1
Ala1 N–Ala95 O	3.2	2.6	2.9	3.1	2.8
Ala1 N–Gly97 O		2.8	3.1		
Ala1 O–Gly94 N	3.2			3.4	3.3
Asn9 $O_{\delta}1$–Glu31 $O_{\epsilon}1$	3.0			2.6	2.5
Asn9 $O_{\delta}1$–Glu31 $O_{\epsilon}2$					3.2
Asn9 $N_{\delta}2$–Gly30 O		3.2	3.4		
Asn9 $N_{\delta}2$–Glu31 $O_{\epsilon}1$	2.9			3.0	
Asn9 $N_{\delta}2$–Glu31 $O_{\epsilon}2$					2.7
Tyr24 OH–Asn43 O		3.1			
Glu28 $O_{\epsilon}1$–Asn44 N				2.9	3.3
Glu28 O–Ser72 O_{γ}			2.8	2.9	2.7
Gly30 N–Ser72 O_{γ}				3.3	
Gly30 O–Ser63 O_{γ}	2.8		2.5		
Thr32 N–Ser63 O_{γ}				3.2	3.1
Thr32 O_{γ}–Ser63 O_{γ}				2.8	2.9
Ser35 O_{γ}–Glu46 $O_{\epsilon}2$				3.3	3.2
Ser35 O_{γ}–Phe100 O	3.3	3.0	2.5	3.0	2.8
Asn36 $N_{\delta}2$–Glu102 $O_{\epsilon}2$					
Asn43 $O_{\delta}1$–Asn83 $N_{\delta}2$		3.1			
Tyr45 O_{η}–Asn83 $N_{\delta}2$	2.6	2.7	2.7		
Asp49 $O_{\delta}1$–Asn98 $N_{\delta}2$		3.3			2.6

[a] Donor–acceptor distances are given in angstrom units. [b] Arni et al. (1988). [c] Kostrewa et al. (1989). [d] Wild type.

the crystal unit cell is similar to that observed for the orthorhombic ($P2_12_12_1$) form of the corresponding wild-type RNase T1·2′-GMP complex (Arni et al., 1987, 1988). Most of the intermolecular contacts observed in the wild-type 2′-GMP complex have their counterparts in at least one or both molecules in the asymmetric unit of the His40Lys RNase T1·2′-GMP crystals (Table II).

The largest structural deviation between the two molecules of the asymmetric unit occurs in the stretch between amino acids Gly47 and Val52 that is part of a loop on the surface of the protein. The structural differences in this region are correlated with changes in the hydrogen-bonding network around Ser51. In molecule 1, Ser51 N and O form hydrogen bonds with two water molecules (2.7 and 3.3 Å, respectively). In molecule 2, no water molecules are visible within hydrogen-bonding distance to Ser51. Instead, highly bent hydrogen bonds are formed between the main-chain atoms Asp49 O and Ser51 N (3.4 Å; 86°) and between Phe50 O and Val52 N (3.5 Å; 94°). The mean temperature factors of the Gly47–Val52 stretch are higher in molecule 2 than in molecule 1 (Figure 2), thus indicating a higher flexibility of this loop in molecule 2. Except for the 47-52 stretch no major differences are observed between the two molecules of the asymmetric unit; the rms deviation between the backbone atoms of both structures is 0.33 Å (Table III).

The overall tertiary structure of His40Lys RNase T1, complexed with 2′-GMP, is essentially identical to that of the corresponding wild-type RNase T1·2′-GMP complex [Arni et al. (1988); see Figure 1]; the structural differences are restricted to the loop regions located on the surface of the enzyme. The rms differences between the backbone atoms of the two mutant molecules in the asymmetric unit and the equivalent backbone atoms of the corresponding wild-type structure are 0.28 and 0.29 Å for molecule 1 and molecule 2, respectively (Table III).

Nucleotide Conformation. In the crystalline complex with His40Lys RNase T1, the 2′-GMP nucleotide adopts a C3′-endo-syn conformation in both molecules of the asymmetric unit (Table IV). The syn conformation around the glycosyl bond is stabilized by a intramolecular hydrogen bond between

Table III: Root Mean Square Differences between RNase T1 Structures[a]

	His40Lys·phosphate	His40Lys·2′-GMP		wt,[e] inhibitor free[b]	wt· vanadate[c]	wt· 2′-GMP[d]
		mol 1	mol 2			
His40Lys·phosphate	X	0.49	0.45	0.21	0.20	0.51
His40Lys·2′-GMP, mol 1	0.17	X	0.33	0.49	0.45	0.28
His40Lys·2′-GMP, mol 2	0.13	0.13	X	0.45	0.41	0.29
wild type, inhibitor free	0.17	0.24	0.20	X	0.15	0.48
wild type·vanadate	0.13	0.21	0.16	0.11	X	0.46
wild type·2′-GMP	0.23	0.14	0.18	0.28	0.26	X

[a] Root mean square distances are given in angstrom units and concern the backbone atoms of the entire protein molecule (above diagonal) and of the catalytic site residues Tyr38, His40 or Lys40, Glu58, Arg77, and His92 (below diagonal). His40Lys RNase T1·phosphate and the inhibitor-free wild-type RNase T1 have been crystallized at pH 7; the other structures have been determined at pH 4–5. [b] Martinez-Oyanedel et al. (1991). [c] Kostrewa et al. (1989). [d] Arni et al. (1988). [e] Wild type.

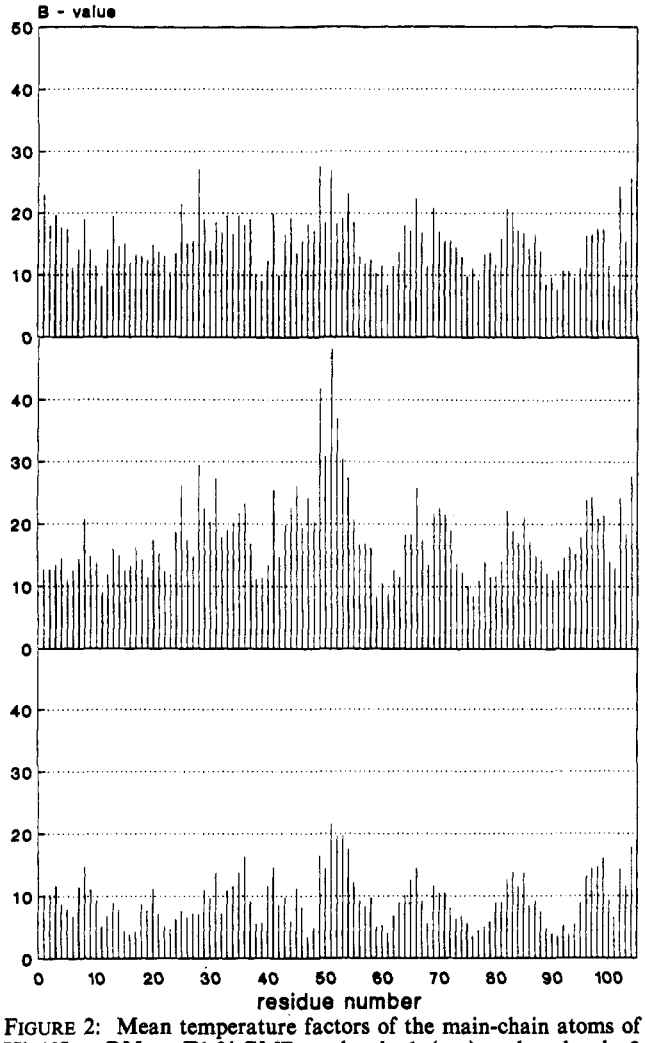

FIGURE 2: Mean temperature factors of the main-chain atoms of His40Lys RNase T1·2′-GMP, molecule 1 (top) and molecule 2 (middle), and of His40Lys RNase T1·phosphate (bottom).

the ribose O5′ and the guanine N3 (3.1 Å for molecule 1 and 3.4 Å for molecule 2). Whereas the syn conformation of 2′-GMP in its complex with RNase T1 is well established (Oshima & Imahori 1971; Takahashi, 1972; Yoshida & Kanae, 1983; Inagaki et al., 1985; Rüterjans et al., 1987; Koepke et al., 1989), the C3′-endo ribose pucker observed in the His40Lys·2′-GMP structure differs significantly from the C2′-endo pucker observed in the corresponding wild type·2′-GMP complex [Arni et al. (1988); Table IV].

Guanine Binding Site. If compared to the corresponding wild-type enzyme (Arni et al., 1988), no significant differences are observed in the guanine binding site of the His40Lys RNase T1·2′-GMP complex (Table V, Figure 3). The hydrogen-bonding potential of the guanine base is saturated by

Table IV: Nucleotide Conformation in Several Ribonuclease T1 Inhibitor Complexes

	His40Lys RNase T1·2′-GMP		RNase T1·2′-GMP[a]
	molecule 1	molecule 2	
Backbone Torsion Angles (deg)			
O5′–C5′–C4′–C3′$_\gamma$	74	30	65
C5′–C4′–C3′–C2′	−163	−145	−94
C4′–C3′–C2′–O2′	−75	−81	−162
C3′–C2′–O2′–P	−80	−91	−122
Glycosyl Torsion Angle (deg)			
O4′–C1′–N9–C4′$_\chi$	34 (syn)	32 (syn)	55 (syn)
Pseudorotation Angles (deg)[b]			
C4′–O4′–C1′–C2′(ν_0)	−3	3	−21
O4′–C1′–C2′–C3′(ν_1)	−27	−25	39
C1′–C2′–C3′–C4′(ν_2)	43	36	−40
C2′–C3′–C4′–O4′(ν_3)	−44	−32	28
C3′–C4′–O4′–C1′(ν_4)	31	19	−5
phase	21 (C3′-endo)	12 (C3′-endo)	168 (C2′-endo)
amplitude	46	36	42

[a] Arni et al. (1988). [b] According to Altona and Sundaralingam (1972).

interactions involving the backbone atoms of Asn43, Asn44, Tyr45, and Asn98 and the Glu46 side chain. The base is further involved in stacking-type interactions with the phenolic side chains of Tyr42 and Tyr45. Tyr45 covers the binding site like a lid.

Catalytic Site Geometry. In contrast to the guanine binding site, the His40Lys mutation causes some differences in the hydrogen bond interactions between the ribose phosphate moiety and the catalytic residues (Table V and Figure 4). The Lys40 side chain is, in both molecules of the asymmetric unit, present in a similar and extended conformation (Figure 5). In molecule 1 of the asymmetric unit, the NH_3^+ group of Lys40 takes part in three hydrogen bonds with Ser36 O, GMP O1P, and GMP O2′ (Table V). In molecule 2 the Lys40 N_ξ shows hydrogen bonding with GMP O1P and GMP O2′ only. In the wild-type RNase T1·2′-GMP complex (Arni et al., 1988) $N_\epsilon 2$ of His40 was observed to form a hydrogen bond with GMP O1P, but not with GMP O2′ or with Ser36 O. In both His40Lys RNase T1 complexes, Glu58 $O_\epsilon 2$ forms a strong hydrogen bond with O3P of the 2′-GMP and a weak hydrogen bond with Arg77 N_ϵ (3.4 and 3.6 Å in the two molecules of the asymmetric unit, respectively). Short hydrogen bonds between caboxylic acid and phosphate oxygens have been found in thermolysin (Holden et al., 1987) and CPDase (Kim et al., 1991) as well. In general, carboxylic acid oxygens are known to form COO–H···O hydrogen bonds as short as 2.4–2.5 Å (Jeffrey & Maluszynska, 1982). In the wild-type structure, both carboxylic acid oxygens were observed to interact exclusively with O3P of 2′-GMP. In contrast to the corre-

Table V: Comparison of the RNase T1·Inhibitor Contacts between the His40Lys RNase T1 Structures and the Corresponding Wild-Type Structures[a]

	His40Lys RNase T1·2′-GMP				wt[e] RNase T1·2′-GMP[b]		His40Lys RNase T1·phosphate		wt RNase T1·vanadate[c]	
	molecule 1		molecule 2							
Tyr38 OH	O1P	2.5	O1P	2.6	O1P	2.7	O3P	3.1	O1V	2.6
Lys40 N_ζ	O2′	3.5	O2′	3.2	NR[d]				NR[d]	
	O1P	3.3	O1P	2.8	NR[d]		O3P	3.3	NR[d]	
His40 $N_\epsilon 2$	NR[d]		NR[d]		O1P	2.8	NR[d]		O3V	3.0
Asn43 N	N7	3.2	N7	2.9	N7	3.2	W175	3.0	W139	2.9
Asn43 $N_\delta 2$	N7	3.4								
Asn44 N	O6	3.0	O6	2.8	O6	2.8				
Tyr45 N	O6	2.9	O6	3.1	O6	2.9	W162	3.1	O43	2.8
Glu46 $O_\epsilon 1$	N1	2.8	N1	2.7	N1	2.7	W116	2.7	N100	2.8
	O6	3.4	O6	3.4						
Glu46 $O_\epsilon 2$	N2	3.1	N2	2.9	N2	2.9	$N_\delta 2$ 99	2.7	$N_\delta 2$ 99	3.0
Glu58 $O_\epsilon 1$					O3P	2.7	O4P	3.2	O4V	2.7
									W175	2.7
Glu58 $O_\epsilon 2$	O3P	2.5	O3P	2.6	O3P	2.4	O2P	3.0	O2V	2.9
									O4V	3.1
Arg77 N_ϵ	O3P	2.9	O3P	2.8			O2P	2.7	O2V	2.6
Arg77 $N_\eta 2$	O3P	3.5	O3P	3.4			O2P	3.1	O2V	3.2
									W199	2.8
His92 $N_\epsilon 2$	O2P	3.0	O2P	3.0			O2P	3.3	O2V	2.8
							O1P	3.3		
Asn98 O	N2	2.7	N2	2.6	N2	2.8	$O_\eta 45$	2.6	$O_\eta 45$	2.6
Asn98 $O_\delta 1$									O1V	3.1

[a] Donor–acceptor distances are given in angstrom units. W represents a water molecule. [b] Arni et al. (1988). [c] Kostrewa et al. (1989). [d] NR, not relevant. [e] Wild type.

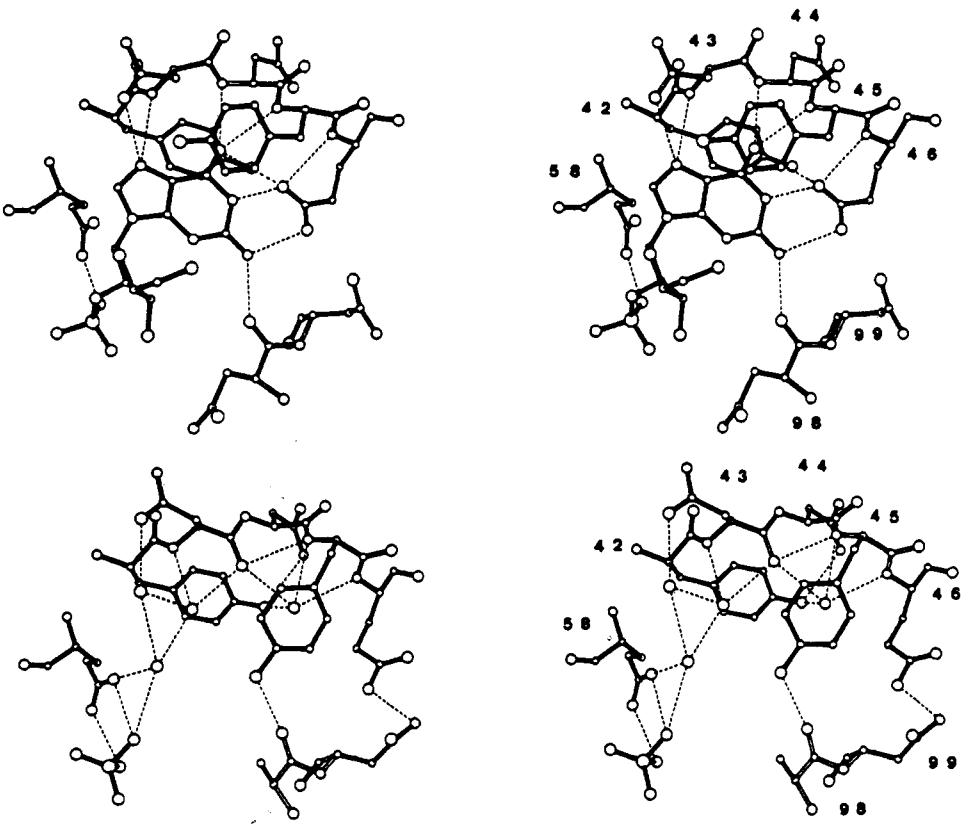

FIGURE 3: Comparison of the guanine binding site of the 2′-GMP complex (top) and the phosphate complex (bottom) of His40Lys RNase T1. In both structures, the residues Tyr42, Asn43, Asn44, Tyr45, Glu46, Glu58, Asn98, and Asn99 are shown.

sponding wild-type structure, Arg77 and His92 makes close contact with the phosphate moiety in the mutant RNase T1 complex (Table V). Similar to the wild-type complex, the phosphate O1P forms hydrogen bonds with Tyr38 and with a water molecule in the mutant structure.

Metal Binding Site. In each molecule of the asymmetric unit of the His40Lys·2′-GMP structure, a calcium ion is coordinated to both carboxylate oxygens of Asp15 and to five water molecules. The observed 7-fold coordination is in the form of a distorted pentagonal bipyramid. This coordination pattern is different from the 8-fold coordination (a dodecahedron with trigonal faces) of an equivalent calcium ion observed in two wild-type RNase T1 structures complexed with 2′,5′-GpG and vanadate (Koepke et al., 1989; Kostrewa et al., 1989). The reason for this difference in calcium coordination is not clear.

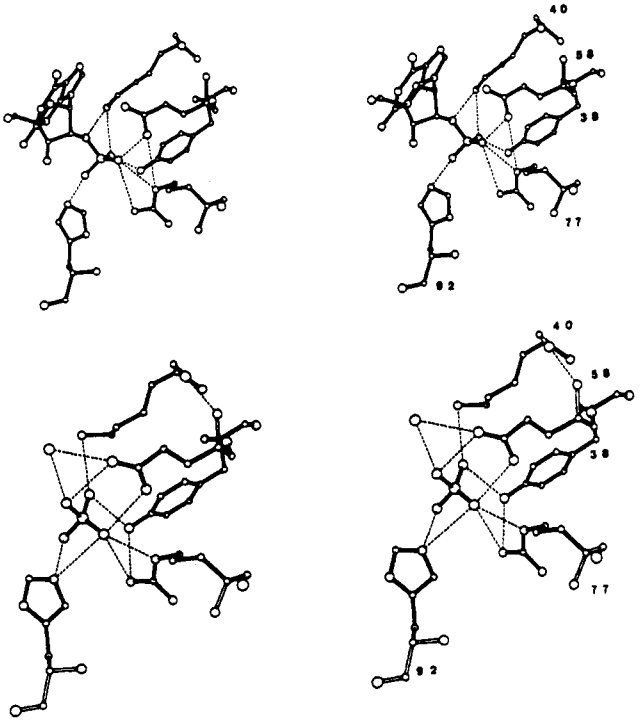

FIGURE 4: Stereo drawing of the active site residues Tyr38, Lys40, Glu58, Arg77, and His92 of His40Lys RNase T1 complexed with 2′-GMP (top) and with phosphate (bottom).

Structure of His40Lys RNase T1·Phosphate

Overall Structure. The structure of His40Lys RNase T1, crystallized without inhibitor, contains a tetrahedral anion in the active site, which we believe to be a phosphate. The shape of the electron density fits a phosphate as well as a sulfate anion (Figure 6). However, phosphate was used at high concentrations during the purification of the protein and probably persisted during crystallization. The calcium concentration in the crystallization buffer is too low to precipitate the phosphate. Therefore a phosphate was fitted in the difference density and refined with bond and angle restraints. The final atomic coordinate set contains 772 protein atoms, 5 phosphate atoms, and 115 water molecules in fully occupied positions. Five protein atoms in the side chains of Lys25 (C_γ, C_δ, C_ϵ, and N_ξ) and Val78 ($C_\gamma 2$) are present in two alternate positions. Lys25 is situated on the surface of the protein, and its two conformations are stabilized by hydrogen bonds between N_ξ and Glu28 and Asp29, respectively. Val78 lies in a hydrophobic cavity in the protein and occupies two positions which are related by a rotation around the C_α–C_β bond. The electron densities for all amino acids except for the Asn98 side chain were clearly visible in the $2F_o - F_c$ map. The atomic coordinates and temperature factors have been deposited in the Brookhaven Protein Data Bank.

The crystals of His40Lys RNase T1·phosphate were near-isomorphous with the corresponding vanadate containing wild-type RNase T1. Although some minor differences occur in the intermolecular contacts, the packing of His40Lys RNase T1·phosphate is very similar to that observed for the corresponding wild-type RNase T1·vanadate [Kostrewa et al., (1989); Table II].

If the His40Lys RNase T1 is compared to the corresponding wild-type RNase T1 (Kostrewa et al., 1989), we find that the global structure of the protein is conserved. The rms difference between the backbones of the two structures is 0.20 Å. The main differences are found in residues on the surface of the enzyme, in the loop between residues 44 and 48, and between residues 94 and 100. Both loops have moved toward each other in the His40Lys mutant, thus strengthening the hydrogen bonds between $O_\epsilon 1$ of Glu46 and $N_\delta 2$ of Asn99 (3.0 → 2.7 Å) and between O_η of Tyr 45 and Asn98 O (3.4 → 2.6 Å). These stronger interactions could explain the lower temperature factors of both regions in the mutant structure, if compared to the corresponding wild-type RNase T1 [see Figure 2 and Kostrewa et al. (1989)].

Guanine Binding Site. The guanine binding site residues Tyr42, Asn43, and Asn44 take similar positions in the phosphate-containing His40Lys RNase T1 if compared to the vanadate-containing structure of wild-type RNase T1 [Table V; Kostrewa et al. (1989)]. In both structures the Asn43 peptide carbonyl group and the Tyr45 side chain are oriented to point into the guanine binding site (Figure 3). Two water molecules occupy the guanine binding site in the guanine-free His40Lys RNase T1, forming hydrogen bonds to Tyr42 O_η, Asn43 O, Tyr45 N, and Asn46 N and to Asn43 O and N, respectively. The positions of Tyr45 and Glu46 are slightly different in the His40Lys RNase T1 structure if compared to the wild-type·vanadate complex. Tyr45 is turned toward the phosphate. The side chain of Glu46 is turned toward the surface of the protein and has a water molecule bound to it. Despite these minor differences, the general conformation of the binding site residues is similar to all structures without a bound guanosine inhibitor (Kostrewa et al., 1989; Martinez-Oyanedel et al., 1991).

Catalytic Site Geometry. The phosphate moiety in the catalytic site of the refined structure of His40Lys RNase T1 has a distorted tetrahedral geometry with a mean P–O bond length of 1.52 Å; the O2–P–O4 angle is the smallest (96°) and the O2–P–O3 angle is largest (127°). The other O–P–O angles range between 102° and 109°. The tetrahedral vanadate in the active site of the wild-type enzyme (Kostrewa et al., 1989) is even more distorted. Here the O2–V–O4 angle is 92°, and the O2–V–O3 angle is 130°. The other O–V–O angles vary from 93 to 124°. More favorable interactions with the catalytic residues may compensate for the observed distortion of the tetrahedral phosphate. Westheimer (1968) proposed a model for the transition state where the pentacovalent phosphorus is the center of a trigonal bipyramid. Three equatorial oxygens are at 120° to each other and at 90° to the apical positions. Because enzymes tend to stabilize the transition-state conformation rather than the ground-state conformation of the substrates, it would appear that the tetrahedral phosphate anion in the RNase T1 active site is distorted toward the trigonal bipyramidal transition state.

The phosphate anion in the His40Lys RNase T1 structure occupies a position and orientation similar to that observed for the tetrahedral vanadate in the wild-type enzyme (Kostrewa et al., 1989); the phosphate forms equivalent hydrogen bonds with the residues Tyr38, Lys40, Glu58, and Arg77 (Table V, Figure 4). In the mutant structure, Lys40 N_ξ forms a hydrogen bond with a phosphate oxygen which corresponds to the hydrogen bond between His40 $N_\epsilon 2$ and a vanadate oxygen in the wild-type structure. In both the mutant and the wild-type RNase T1 structure, Glu58 forms two hydrogen bonds with two of the phosphate oxygens. These hydrogen bonds indicate that, in the presence of a phosphate, Glu58 is protonated at pH 7. This is in agreement with earlier potentiometric titration data of RNase T1 and its complex with 2′-GMP (Iida & Ooi, 1969), confirming that it is the Glu58 carboxylate group that increases its pK_a upon inhibitor binding. In contrast to the RNase T1·vanadate structure (Kostrewa et al., 1989), the Asn98 side chain [which has been implicated in subsite

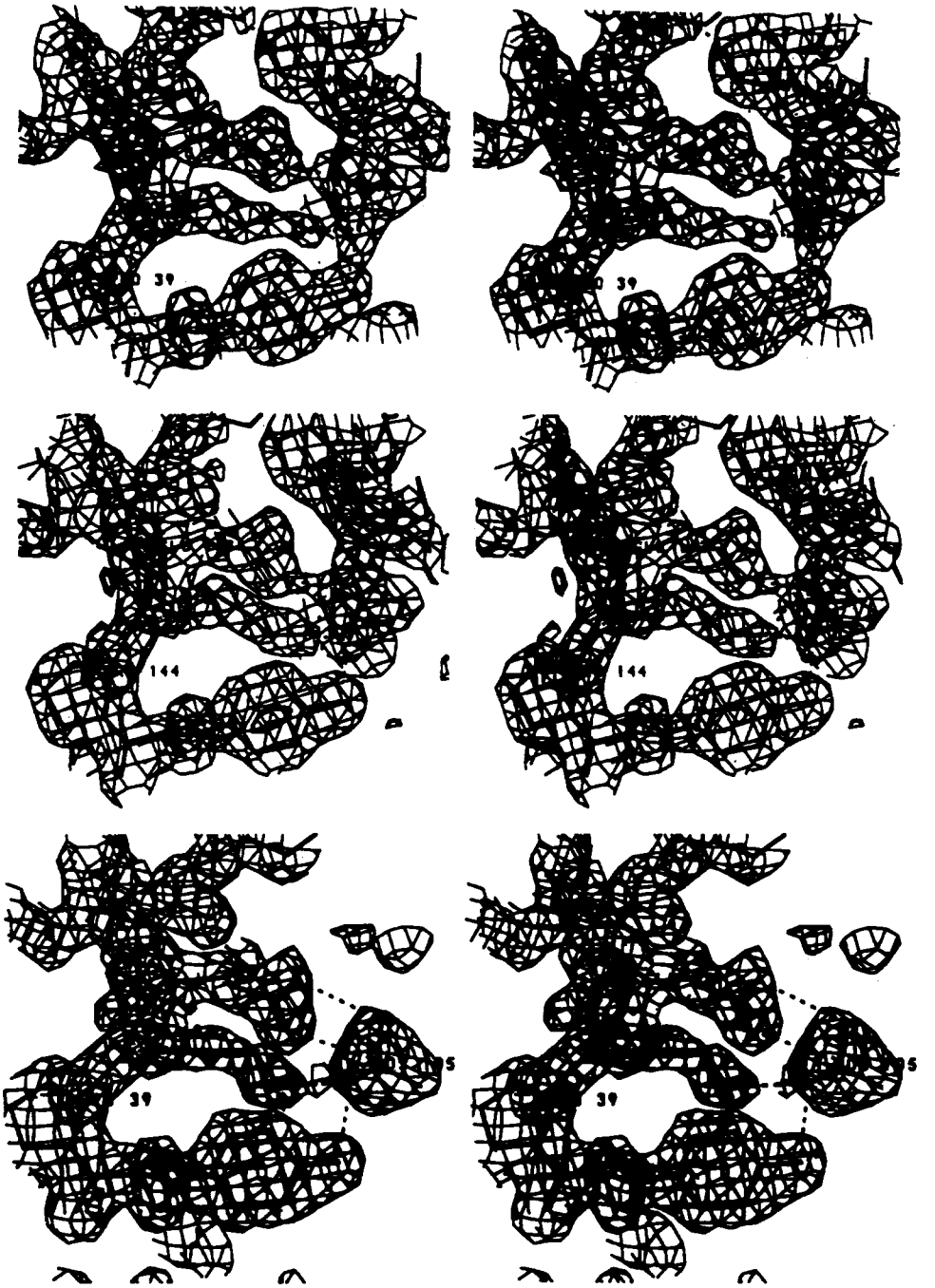

FIGURE 5: $2F_o - F_c$ electron density in the active site of (a, top) molecule 1 and (b, middle) molecule 2 of His40Lys RNase T1·2′-GMP and (c, bottom) of the phosphate complex of His40Lys RNase T1.

interactions (Steyaert et al., (1991b)] is not visible in the electron density map. This could possibly be associated with the observed rearrangement of the 94–100 loop, which distances the Asn98 from the phosphate.

Calcium Binding Site. A calcium ion is coordinated to the two oxygen atoms of Asp15 and to six water molecules. The eight oxygen atoms form a dodecahedron with trigonal faces, also found in previous RNase T1 structures (Koepke et al., 1989; Kostrewa et al., 1989; Martinez-Oyanedel et al., 1991).

DISCUSSION

Structure of His40Lys RNase T1. The structure of the His40Lys RNase T1 mutant was determined with and without the specific inhibitor 2′-GMP. The complex with 2′-GMP crystallized at pH 4.2 in the monoclinic space group $P2_1$ with two molecules in the asymmetric unit. The guanosine-free structure, which contains a phosphate in the active site, crystallized in space group $P2_12_12_1$ at pH 7.0.

In Table III the overall structures of the three His40Lys RNase T1 molecules are compared with the relevant wild-type structures which were determined previously. The highest rms differences are observed if guanine-containing structures are compared to guanine-free structures. This is mainly due to a reorganization of the guanine binding site upon binding of 2′-GMP (Kostrewa et al., 1989). This rearrangement is also observed if the 2′-GMP-containing His40Lys structures are compared to the phosphate-containing His40Lys structure (see Results). The small rms deviations between all couples of either guanine-containing or guanine-free structures, respectively, illustrate that the overall structure and the active site geometry are not significantly affected by the mutation

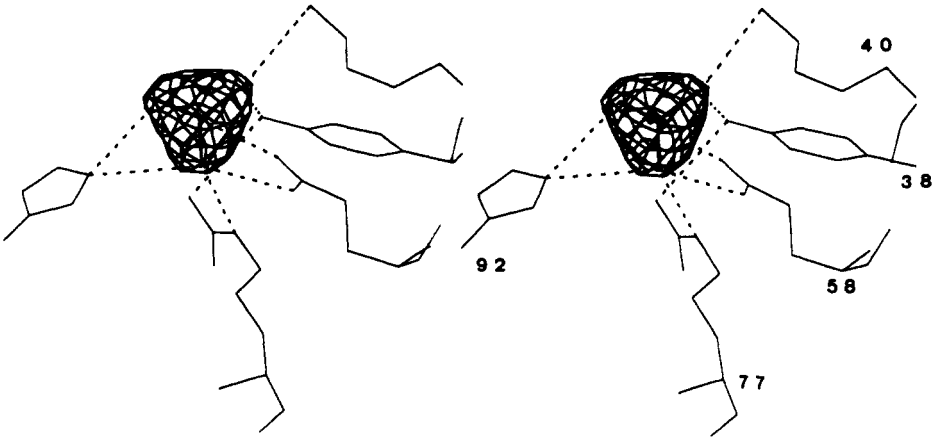

FIGURE 6: $F_o - F_c$ difference density of the phosphate anion in His40Lys RNase T1·phosphate. The map was calculated after 12 refinement cycles with the final coordinate set from which the phosphate was deleted.

of His40 to Lys, the shift of pH from 4–5 to 7, or the change of space group from $P2_12_12_1$ to $P2_1$.

The Lys40 side chain is clearly visible in the electron density map of the phosphate-containing and of both 2′-GMP-containing His40Lys T1 structures. Although the conformation of Lys40 is always extended, the positions of the side-chain atoms vary in the different His40Lys structures, suggesting a certain flexibility. This is consistent with the relatively high temperature factors of Lys40 (Figure 2). The lysine side chain fits loosely in a cylindrical space, and its terminal amino group forms a hydrogen bond to a phosphate oxygen in all three mutant structures.

In contrast to the wild type·2′-GMP complex (Arni et al., 1988), all amino acids which have been implicated in catalytic turnover [i.e., Tyr38, Lys40, Glu58, His92, and Arg77 (Pace et al., 1991; Steyaert et al., 1991b)] are in hydrogen-bonding distance to the phosphate moiety of 2′-GMP in its complex with His40Lys RNase T1 (Table V). This notable difference could be correlated with the C3′-endo-syn conformation of 2′-guanilic acid, which is stabilized by a Lys40 N_ζ–GMP O2′ hydrogen bond observed in both molecules of the asymmetric unit (Table V). The C3′-endo sugar pucker differs from the C2′-endo pucker found in the wild-type RNase T1·2′-GMP crystal structure (Arni et al., 1988). NMR solution studies indicate that 2′-GMP and 3′-GMP bind in a 3′-endo-syn conformation (Inagaki et al., 1985). The observation that the nature of the interactions of most catalytic residues with the phosphate moiety changes with the 2′-endo to 3′-endo pucker transition suggests that the sugar conformation has major implications on the catalyzed reaction.

Catalytic Function of His40. His40 has been identified as a key catalytic residue for the RNase T1 catalyzed transesterification reaction. His40Ala and His40Asp mutants retain less than 0.1% of the wild-type activity toward RNA (Steyaert et al., 1990). In addition, the His40 side chain contributes about 1.5 kcal/mol toward ground-state binding (Steyaert et al., 1991a). The His40Lys mutant however retains 3.1% of the activity of the wild-type enzyme, indicating that Lys40 partially compensates for the removal of the protonated His40 imidazole in the wild-type enzyme.

All structural data on the His40Lys mutant indicate that the His40Lys mutation is highly conservative. We observe a Lys40 N_ζ–O(phosphate) hydrogen bond in all the His40Lys structures which has its counterpart in the His40 N_ϵ–O(phosphate) interaction in the corresponding wild-type structures. In addition, the other active site residues Tyr38, Glu58, Arg77, and His92 occupy very similar positions in the His40Lys RNase T1 structures if compared to the corresponding wild-type enzymes. These structural observations are consistent with kinetic data (Osterman & Waltz, 1978, Steyaert et al., 1990) and indicate that (1) Glu58 functions as a base catalyst in both the wild-type enzyme and His40Lys RNase T1 and that (2) histidine and lysine share a feature that is essential for catalysis; both histidine and the more flexible lysine contain a positive charge which interacts with the phosphate moiety of the substrate.

Anslyn and Breslow (1989) showed that the first step in the imidazole-catalyzed transesterification of 3′,5′-UpU consists of the protonation of the phosphodiester. The proton placed on the phosphate plays the role of an electrophilic catalyst, increasing the electrophilicity of the phosphorus. The protonation allows for a more facile attack by the 2′-OH and stabilizes the second negative charge that develops during transition-state formation. In wild-type RNase T1 His40 could protonate the phosphate diester. It is, however, unlikely that Lys40 in His40Lys RNase T1 protonates the phosphate. It can instead activate the phosphate and stabilize the dianionic transition state through hydrogen-bonding and electrostatic interactions. The transition state could further be stabilized through interactions with Tyr38 and Arg77. Short contacts between the phosphate anion and Tyr38 and Arg77 are observed in the three His40Lys RNase T1 structures described herein.

ACKNOWLEDGMENT

We thank Maria Vanderveken for excellent technical assistance.

REFERENCES

Altona, C., & Sundaralingam, M. (1972) *J. Am. Chem. Soc. 94*, 8205–8212.

Anslyn, E., & Breslow, R. (1989) *J. Am. Chem. Soc. 111*, 4473–4482.

Arni, R., Heinemann, U., Maslowska, M., Tokuoka, R., & Saenger, W. (1987) *Acta Crystallogr. B43*, 548–554.

Arni, R., Heinemann, U., Tokuoka, R., & Saenger, W. (1988) *J. Biol. Chem. 263*, 15358–15368.

Baker, E. N., & Hubbard, R. E. (1984) *Prog. Biophys. Mol. Biol. 44*, 97–179.

Eckstein, F., Schulz, H. H., Rüterjans, H., Haar, W., & Maurer, W. (1972) *Biochemistry 11*, 3507–3512.

Finzel, B. C. (1987) *J. Appl. Crystallogr. 20*, 53–55.

Heinemann, U., Saenger, W. (1982) *Nature 299*, 27–31.

Heinemann, U., & Saenger, W. (1983) *J. Biomol. Struct. Dyn. 1*, 523–538.

Hendrickson, W. A. (1985) *Methods Enzymol. 115*, 252–270.
Hendrickson, W. A., & Konnert, J. H. (1980) in *Computing in Crystallography* (Diamond, R., Ramaseshan, S., & Venkatesan, K., Eds.) pp 13.01–13.23, Indian Academy of Sciences, Bangalore, India.
Hill, C., Dodson, G., Heinemann, U., Saenger, W., Mitsui, Y., Nakamura, K., Borisov, S., Tischenko, G., Polyakov, K., & Pavlovsky, S. (1983) *Trends Biochem. Sci. 8*, 364–369.
Holden, M. H., Tronrud, D. E., Monzingo, A. F., Weaver, L. H., Matthews, B. W. (1987) *Biochemistry 26*, 8542–8553.
Iida, S. & Ooi, T. (1969) *Biochemistry 8*, 3897–3902.
Inagaki, F., Shimida, J., & Miyazawa, T. (1985) *Biochemistry 24*, 1013–1020.
Jeffrey, G. A., & Maluszynska, H. (1982) *Int. J. Biol. Macromol. 4*, 173–185.
Jones, T. A. (1978) *J. Appl. Crystallogr. 11*, 268–272.
Jones, T. A. (1985) *Methods Enzymol. 115*, 157–171.
Kim, H., & Lipscomb, W. N. (1991) *Biochemistry 30*, 8171–8180.
Koepke, J., Maslowska, M., Heinemann, U., & Saenger, W. (1989) *J. Mol. Biol. 206*, 475–488.
Kostrewa, D., Choe, H.-W., Heinemann, U., & Saenger, W. (1989) *Biochemistry 28*, 7592–7600.
Martinez-Oyanedel, J., Choe, H. W., Heinemann, U., & Saenger, W. (1991) *J. Mol. Biol. 222*, 335–352.
Nishikawa, S., Morioka, H., Kim, H. J., Fuchimura, K., Tanaka, T., Uesugi, S., Hakoshima, T., Tomita, K., Ohtsuka, E., & Ikehara, M. (1987) *Biochemistry 26*, 8620–8624.
Oshima, T., & Imahori, K. (1971) *J. Biochem. (Tokyo) 70*, 197–199.
Osterman, H. L., & Walz, F. G., Jr. (1978) *Biochemistry 17*, 4124–4130.
Pace, N., Heinemann, U., Hahn, U., & Saenger, W. (1991) *Angew. Chem. 30*, 343–454.
Rüterjans, H., Hoffman, E., Schmidt, J., & Simon, J. (1987) in *Metabolism and Enzymology of Nucleic Acids Including Gene Manipulations* (Zelinka, J., & Balan, J., Eds.) Vol. 6, pp 81–96, Slovak Academy of Sciences, Bratislava, Czechoslovakia.
Sato, K., & Egami, F. (1957) *J. Biochem. 44*, 753–767.
Sheriff, S. (1987) *J. Appl. Crystallogr. 20*, 55–57.
Steyaert, J., Hallenga, K., Wyns, L., & Stanssens, P. (1990) *Biochemistry 29*, 9064–9072.
Steyaert, J., Wyns, L., & Stanssens, P. (1991a) *Biochemistry 30*, 8661–8665.
Steyaert, J., Haikal, A. F., Wyns, L., & Stanssens, P. (1991b) *Biochemistry 30*, 8666–8670.
Sussman, J. L., Holbrook, S. R., Church, G. M., & Kim, S.-H. (1977) *Acta Crystallogr. A33*, 800–804.
Takahashi, K. (1972) *J. Biochem. 72*, 1469–1482.
Usher, D. A. (1969) *Proc. Natl. Acad. Sci. U.S.A. 62*, 661–667.
Westheimer, F. H. (1968) *Acc. Chem. Res. 1*, 70–78.
Yoshida, H., & Kanae, H. (1983) *Biochem. Biophys. Res. Commun. 114*, 88–92.

Registry No. His, 71-00-1; Lys, 56-87-1.